Quantum Couplings and Magnetic Properties of $CoCr_xFe_{2-x}O_4$ ($0 < x < 1$) Spinel Ferrite Nanoparticles Synthesized with Reverse Micelle Method

Man Han, Christy R. Vestal, and Z. John Zhang*

School of Chemistry and Biochemistry, Georgia Institute of Technology, Atlanta, Georgia 30332-0400

Received: July 8, 2003; In Final Form: November 13, 2003

Spinel ferrite $CoCr_xFe_{2-x}O_4$ nanoparticles over a compositional range $0 < x < 1$ were synthesized using a reverse micelle microemulsion method. This method provided excellent control over the composition and gave a reasonable size distribution. Upon increased Cr substitution, the blocking temperature, saturation magnetization, remnant magnetization, and coercivity were all found to decrease. The compositional influence upon the magnetic properties is consistent with the effects on the magnetocrystalline anisotropy energy by weakened coupling between electron spin and the angular momentum of electron orbital (L−S coupling). The results from size dependent magnetic studies on the nanoparticles with a composition of $CoCr_{0.5}Fe_{1.5}O_4$ were found to agree well with the Stoner−Wohlfarth model.

Introduction

Research into the synthesis and characterization of magnetic materials has been conducted for more than a century. The importance of magnetic materials in our daily life ranges from electric motors and magnetic storage devices to Brio toy trains. Recently, the ability to produce nanometer-scale magnetic materials has opened new applications for magnetic materials such as magnetic media for high-density recording, magnetocaloric refrigeration, contrast enhancement in magnetic resonance imaging (MRI), and magnetically guided drug delivery.[1−4] Preparing nanoparticles for such applications requires better understanding and control over the magnetic properties such as superparamagnetism in the nanoparticulate magnetic systems. Moreover, systematic studies of magnetic nanoparticles enable us to advance our understanding to the fundamentals of magnetism such as quantum origins of magnetic anisotropy and coercivity.

Spinel ferrite is a very informative crystal system for understanding and designing the magnetic properties of nanoparticles through chemical manipulations.[5] Spinel structure, generally denoted by the formula AB_2O_4, contains two cation occupancy sites: the A sites have a tetrahedral coordination by oxygen, while the B sites are octahedrally coordinated. Spinel ferrite, MFe_2O_4 (M = Mn, Fe, Co, Zn, Mg, etc.) is a ferrimagnetic system. Based upon the simple collinear model, the magnetic moments of all the cations at A sites align parallel with each other. The magnetic moments of the cations at the B sites also align parallel with each other. Between the magnetic moments at A and B sites, the alignments are antiparallel. The exchange coupling between A and B sites, J_{A-B}, usually is stronger than the exchange couplings between A sites, J_{A-A}, or between B sites, J_{B-B}. In addition to these exchange couplings, the coupling between the angular momentum of electron orbital and electron spin (L−S coupling) could also exist at each magnetic cation site. Certainly, the strength of quantum couplings such as exchange and L−S couplings will vary with the change of cations in chemical composition and with different cation distribution between the A and B sites. Consequently, the magnetic properties of nanoparticles will change with changing quantum couplings at the atomic level.

The quantum couplings between electron spin and orbital angular momentum are very complicated and thus far are not fully understood. Nevertheless, such couplings can provide invaluable guidance to qualitatively understanding and designing the magnetic properties of nanoparticles. The superparamagnetic transitions in spinel ferrite nanoparticles of $CoFe_2O_4$, $MgFe_2O_4$, and $MnFe_2O_4$ show very interesting connections with the L−S couplings. $CoFe_2O_4$ nanoparticles normally become superparamagnetic at a relatively higher temperature, which is known as blocking temperature, T_b. For instance, 10 nm $CoFe_2O_4$ nanoparticles have a blocking temperature around 300 K.[5] However, the blocking temperature of $MgFe_2O_4$ nanoparticles with similar size is around 130 K, which is similar to the blocking temperature of ∼150 K in 10 nm $MnFe_2O_4$ nanoparticles.[6] In all these spinel ferrite nanoparticles, the cation distribution is comparable. Since Mg^{2+} has no unpaired electrons and Mn^{2+} has five unpaired electrons, similar blocking temperatures in $MgFe_2O_4$ and $MnFe_2O_4$ nanoparticles may suggest that the Fe^{3+} cations predominately determine the magnetic properties of these nanoparticles. Partial substitution of Fe^{3+} cations with another metal cation could provide some insights into the correlations between the quantum couplings and magnetic properties of nanoparticles.

$CoCr_xFe_{2-x}O_4$ spinel ferrite nanoparticulate system offers an opportunity to study the roles of Fe^{3+} in spinel ferrites through the variation of Cr^{3+} ion concentration. Cr^{3+} ions usually occupy the octahedral B sites in spinels.[7] A decrease in total magnetic moment at B sites is expected as Cr^{3+} with a magnetic moment of $3\mu_B$ replaces the stronger Fe^{3+} ($5\mu_B$) cation. Cr^{3+} ion has an electron configuration of $t_{2g}^3e_g^0$ in spinel structure, which theoretically has a relatively large orbital angular momentum. The Fe^{3+} ion at the B site has $t_{2g}^3e_g^2$ electron configuration in spinel structure, which theoretically has a zero orbital angular momentum. Therefore, the substitution of Fe^{3+} by Cr^{3+} in $CoCr_xFe_{2-x}O_4$ nanoparticles should also offer certain information on the contribution from the orbital angular momentum toward magnetic properties. However, such substitutions can introduce the variation of exchange coupling into this mixed spinel ferrite

* To whom correspondence should be addressed.

10.1021/jp035966m CCC: $27.50
Published on Web 12/17/2003

system. Therefore, the collinear model may not be correct, and triangular or spiral ferrimagnetic arrangement may dominate the magnetic order.[8−10] Cr substitution could be complicated since the exchange couplings between Cr^{3+} ions display a large negative exchange constant (J_{B-B}).[7] A strong negative J_{B-B} interaction favors antiparallel alignment. Although such an arrangement is hindered in mixed spinel ferrites, it could disrupt the parallel alignment of spins on the B site to various extents and lead to spin canting. In the case where $x = 2$ ($CoCr_2O_4$), the antiferromagnetic alignment between A and B sites is completely destroyed and the system displays a screw ordering.[7] When $x = 1$ ($CoCrFeO_4$), magnetic frustration has been observed in bulk samples.[11,12] Therefore, it is also fundamentally interesting to see if the magnetic order has been altered in nanoparticles by Cr substitution.

Although spinel ferrite nanoparticles have been synthesized by a variety of methods such as high-energy ball milling,[13] coprecipitation,[14] and sol−gel method,[15] microemulsion synthesis allows for the formation of high-quality nanoparticles with controllable size and composition through minor adjustments to the synthesis conditions.[16,17] Vestal and Zhang have recently reported the synthesis of $CoCrFeO_4$ nanoparticles using reverse and normal micelle microemulsion procedures.[18] The reverse micelle procedure has resulted in a more repeatable synthesis of similar sized nanoparticles. We report here the synthesis of a series of ∼8 nm $CoCr_xFe_{2-x}O_4$ spinel ferrite nanoparticles with composition $0 < x < 1$ using reverse micelle microemulsion methods. Magnetic properties have been characterized as a function of chromium substitution. Samples with composition $CoCr_{0.5}Fe_{1.5}O_4$ were further characterized as a function of particle size.

Experimental Section

Nanoparticle Synthesis. $CoCr_xFe_{2-x}O_4$ nanoparticles were prepared by a reverse micelle microemulsion method. Aqueous solutions of $CoCl_2 \cdot 6H_2O$ (Fisher, 98%), $CrCl_3 \cdot 6H_2O$ (Aldrich, 98+%), $Fe(NO_3)_3 \cdot 9H_2O$ (Alfa Aesar, 98+%), and dodecylbenzenesulfonate (Aldrich, 98%) were mixed and stirred for ∼1 h. A large volume of toluene (JT Baker, ACS grade) was added to the mixture and stirred overnight to form the reverse micelles. Methylamine (Acros, 40% in water) was added to the micelle solution, stirred for ∼2 h, and then refluxed for ∼4 h. Following removal of ∼3/4 volume of toluene by distillation, the resulting brown product was washed with ethanol and water to remove excess surfactant. The nanoparticles were collected using centrifugation. The sample was annealed in air at a ramping rate of 1 °C/min and held at 600 °C for 20 h and became a fine black powder. To vary the composition, appropriate molar ratios of the metal cation solutions were used. Variable sized nanoparticles were prepared by adjusting the water-to-toluene ratio for samples with composition $CoCr_{0.5}Fe_{1.5}O_4$.

Instrumentation. X-ray diffraction data were collected with a Bruker D8 ADVANCE X-ray diffractometer over a 15°−85° 2θ range. Particle sizes were determined from the average peak broadening of the five strongest Bragg peaks by using the commercial program TOPAS. Transmission electron microscopy (TEM) studies were performed using a JEOL 100C instrument operating at 100 kV. Particle size distributions were determined by manually counting over 100 particles in TEM micrographs. Neutron diffraction studies were conducted on the Special Environment Powder Diffractometer (SEPD) using the Intense Pulse Neutron Source at Argonne National Laboratory.[19] A Quantum Design MPMS-5S SQUID magnetometer was used to perform magnetic measurements. Magnetic susceptibility measurements were performed from 5 to 650 K under a 100 G field, while field dependent hysteresis measurements were measured at 5 K in applied fields up to 5 T. Particles were immobilized in eicosane ($C_{20}H_{42}$, Aldrich) for the hysteresis measurements.

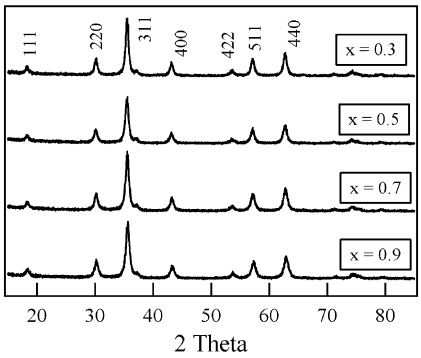

Figure 1. X-ray diffraction patterns of ∼8 nm $CoCr_xFe_{2-x}O_4$.

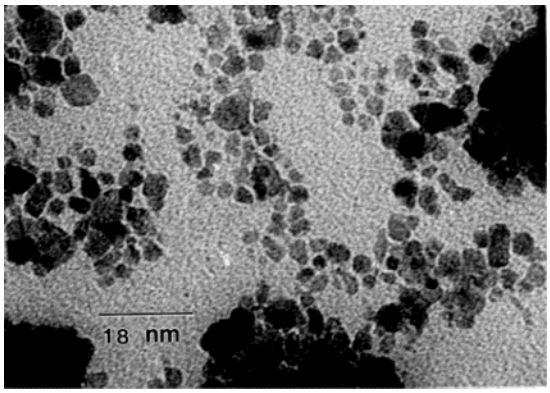

Figure 2. TEM micrograph of $CoCr_{0.3}Fe_{1.7}O_4$ nanoparticles with a size of 8.0 ± 1.5 nm.

Results and Discussion

X-ray diffraction patterns shown in Figure 1 indicate that pure spinel phase $CoCr_xFe_{2-x}O_4$ nanoparticles are synthesized using the reverse micelle microemulsion method. Such a crystalline phase appears only after the thermal treatment at 600 °C. Average particle size was ∼8 nm determined by the Scherrer equation using the Bragg peak broadening data. TEM studies confirmed particle sizes (Figure 2) and also yielded a size distribution of 19%. Table 1 shows excellent agreement between the theoretical Cr composition calculated from the molar ratio in reagents and actual composition in nanoparticles determined by elemental analysis using inductively coupled plasma atomic emission spectroscopy (ICP-AES). The ratio of Co versus the sum of Fe and Cr has been maintained as 1 to 2. Mössbauer spectroscopic studies have proved that Fe cation in the nanoparticles has a +3 oxidation state, which suggests that the chemical composition of the nanoparticles has a stoichiometry close to standard spinel. The consistent trends in the magnetic properties of these nanoparticles also indicate the absence of significant defects from cation vacancy since the randomness of defect chemistry would have had significant effects on the magnetic trends of these nanoparticles.

The Cr occupancy at sublattices in spinel unit cell has been determined from neutron diffraction studies. A neutron diffraction pattern is shown in Figure 3 for 10 nm $CoCrFeO_4$ nanoparticles at room temperature. The Rietveld refinement using the GSAS program shows that the magnetic sublattices have an antiferromagnetic order. Although Co and Fe distribute

TABLE 1: Elemental Analysis of $CoCr_xFe_{2-x}O_4$ Nanoparticles

theoretical Cr percentage	5	10	15	20	25	30	35	40	45
Cr percentage from ICP-AES	5.1	9.7	14.6	20.4	24.6	29.5	34.9	41.2	45.2

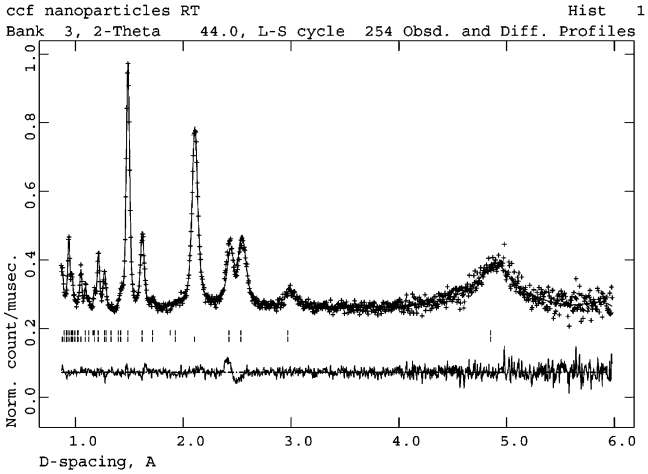

Figure 3. Neutron diffraction pattern of 10 nm $CoCrFeO_4$ nanoparticles at room temperature. The "goodness of fit" χ^2 is 1.44 and $R(f^2)$ for the data fitting is 0.0348. Below the pattern, the first row of the sticks marks the peaks from the magnetic scattering of $CoCrFeO_4$ nanoparticles. The second row of the sticks corresponds to the peaks from the nuclear scattering.

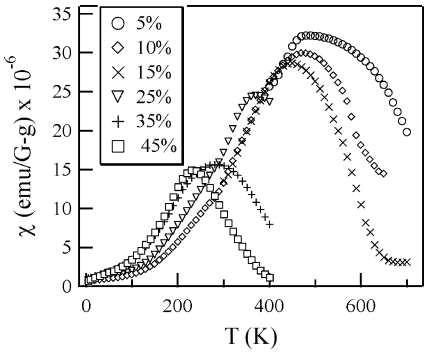

Figure 4. Temperature dependent susceptibility of ~8 nm $CoCr_xFe_{2-x}O_4$ nanoparticles with variable Cr doping under a magnetic field of 100 G.

at both A and B sites, Cr cations occupy only B sites. Regarding the cation occupancy, the formula for the nanoparticles is $(Co_{0.76}Fe_{0.24})[Co_{0.12}Fe_{0.38}Cr_{0.5}]_2O_4$, where the cations in parentheses occupy the tetrahedral A sites and the composition in brackets shows the cation occupancy at the octahedral B sites. The lattice constant for the cubic spinel unit cell is 8.347 Å at room temperature. The average magnetic moment is $1.26\mu_B$ at the A sites and $-1.24\mu_B$ at the B sites.

Figure 4 shows the temperature dependent magnetic susceptibility of $CoCr_xFe_{2-x}O_4$ nanoparticles with varying Cr composition. Generally, the magnetic susceptibility increases slowly as temperature increases and reaches a maximum, which is referred as a blocking temperature (T_b), and then slowly decreases. Figure 5 shows T_b clearly decreases as the Cr doping concentration is increased.

Field dependent magnetization measurements show hysteresis at temperatures below T_b for all compositions. The hysteresis curves at 5 K are displayed in Figure 6 for ~8 nm nanoparticles with various Cr compositions. The saturation magnetization (M_S), the remnant magnetization (M_R), and the coercivity (H_C) all decrease with increasing Cr doping percentage (Figure 7).

A series of $CoCr_{0.5}Fe_{1.5}O_4$ nanoparticles with their mean size range at ~6−11 nm have been obtained by varying the water-to-toluene ratio in the syntheses. The temperature dependent magnetic susceptibility measurement as a function of size is presented in Figure 8 for these nanoparticles. Increasing nanoparticle size results in an increased T_b as shown in the inset. Figure 9 shows the hysteresis behavior at 5 K for these nanoparticles with various mean sizes. An increase in M_S, M_R, and H_C is observed with increasing nanoparticle size (Figure 10).

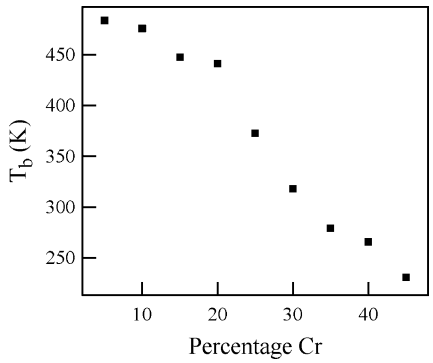

Figure 5. Composition dependence of blocking temperature under a 100 G field.

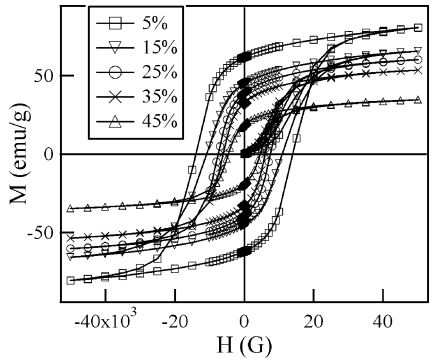

Figure 6. Field dependent magnetization of ~8 nm $CoCr_xFe_{2-x}O_4$ nanoparticles with variable Cr doping.

The magnetic order confirmed by neutron diffraction studies above the blocking temperature unambiguously shows that these magnetic nanoparticulate systems are truly superparamagnetic. The Cr cations indeed have partially replaced the Fe cations at the octahedral sites. The small magnetic moment at the B site suggests that strong B−B couplings may have caused the magnetic dipoles at B sites to be canted, and consequently, the magnetic moment was reduced.

The decrease in the blocking temperature T_b with increasing Cr composition (Figure 5) suggests a decrease of the magnetic anisotropy energy (E_A). The Stoner−Wohlfarth model describes E_A of single domain nanoparticles as

$$E_A = KV \sin^2 \theta \qquad (1)$$

where K is the anisotropy energy constant, V is the volume of the nanoparticle, and θ is the angle between the nanoparticle's easy axis and the applied field direction.[20] The strength of the L−S couplings is reflected in the magnitude of K.[21] The blocking temperature T_b represents the threshold at which thermal activation, k_BT (k_B is the Boltzmann constant), is strong enough to overcome E_A. Above T_b thermal energy and/or an applied magnetic field is sufficient to move the magnetization

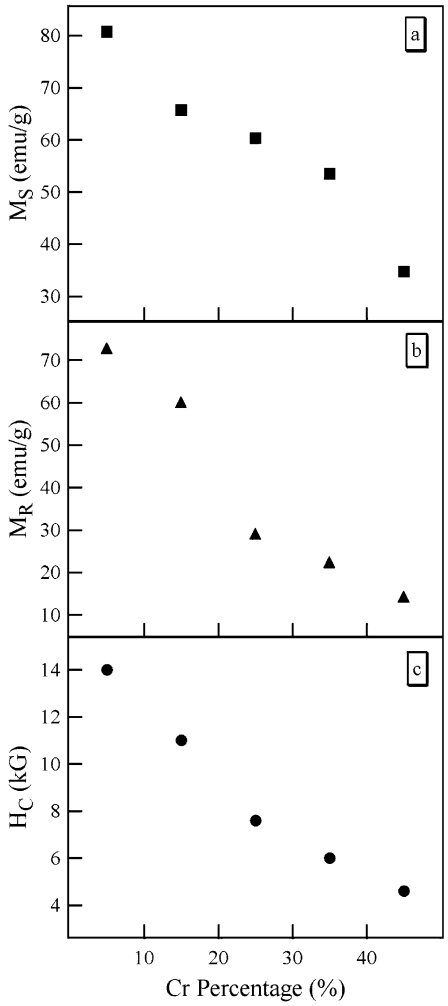

Figure 7. (a) Composition dependence of saturation magnetization for $CoCr_xFe_{2-x}O_4$ nanoparticles. (b) Composition dependence of remnant magnetization. (c) Composition dependence of coercivity.

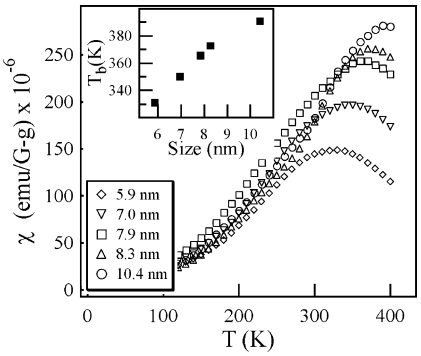

Figure 8. Temperature dependent susceptibility of $CoCr_{0.5}Fe_{1.5}O_4$ nanoparticles with variable sizes under a 100 G field. Inset shows the size dependence on the blocking temperature.

direction of the nanoparticle away from its easy axis and the particle displays superparamagnetism. The observed decrease in T_b upon increasing the Cr concentration implies a reduction in E_A resulting from weakened L−S couplings (weaker K). Incorporation of more Cr ions into the B sites weakens the L−S couplings further, probably due to the weaker magnetic moment of Cr^{3+} compared to Fe^{3+}. Such results suggest that the L−S couplings in Cr^{3+} do not benefit from its relatively large orbital angular momentum. On the other hand, Co^{2+} with a $t_{2g}^5e_g^2$ electron configuration in spinel has very strong L−S coupling even though it has the same number of unpaired electrons and

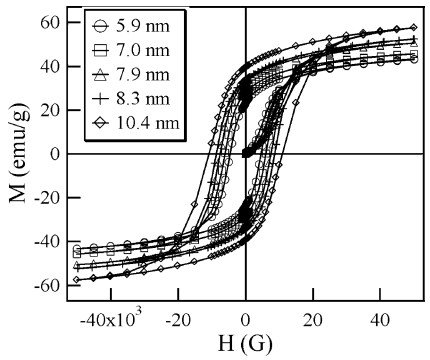

Figure 9. Field dependent magnetization of $CoCr_{0.5}Fe_{1.5}O_4$ nanoparticles with varying size.

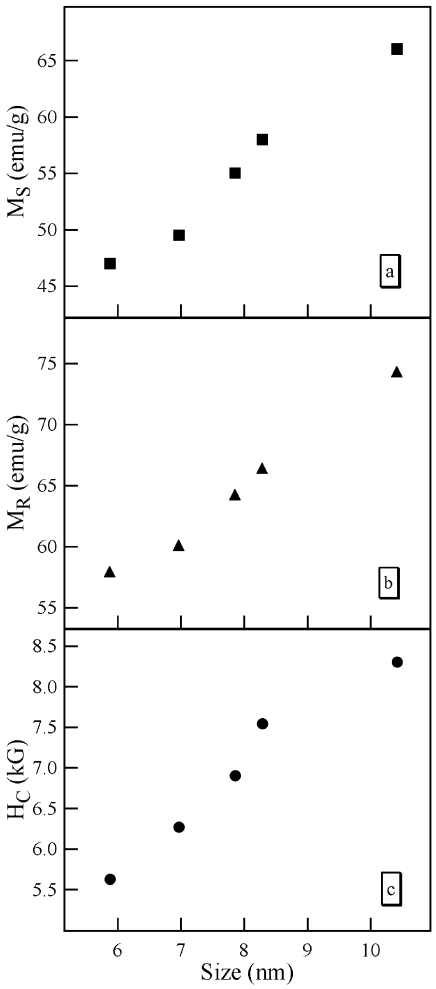

Figure 10. (a) Size dependence of saturation magnetization for $CoCr_{0.5}Fe_{1.5}O_4$ nanoparticles. (b) Size dependence of remnant magnetization. (c) Size dependence of coercivity.

the same theoretical orbital angular momentum as the Cr^{3+} cation. The great difference in magnetic behavior between Co^{2+} and Cr^{3+} cations in spinel ferrite nanoparticles may offer some insights into the magnetic quantum interactions at the atomic level.

The observed decrease in coercivity upon Cr doping (Figure 7c) can be explained by a reduction of L−S coupling strength as well. The magnitude of the coercivity can be considered as a measure of the magnetic field strength that is required at the given temperature to overcome the anisotropy energy barrier in order to change the magnetization direction in a material.[21] The lowering of the coercivity upon doping agrees with a

reduction of the magnetization reversal energy barriers. The magnitude of the energy barriers is lowered through a reduction of the magnetic couplings resulting from the weaker magnetic moment of Cr^{3+}. The observed decrease in the saturation magnetization and remnant magnetization (Figure 7a,b) upon incorporation of more Cr is consistent with a decrease in the net magnetic moment as a result of substitution of Fe^{3+} ($5\mu_B$) with magnetically weaker Cr^{3+} ($3\mu_B$) and increasing canting of magnetic dipoles because of the strong negative J_{B-B} contribution.

Size Dependent Characterization of $CoCr_{0.5}Fe_{1.5}O_4$. The results of T_b as a function of size (Figure 8) show excellent agreement with the size dependence of the magnetocrystalline anisotropy energy (E_A). According to eq 1, E_A increases as the size of the particle (V) increases. Larger sized particles require higher temperatures to overcome a higher E_A, and our observed increase in T_b as a function of particle size is in accordance with the Stoner−Wohlfarth theory. The results from hysteresis measurements show that the magnetic moment, remnant magnetization, and coercivity increase as particle size increases (Figure 10). This too is consistent with an increase in the magnitude of the magnetocrystalline energy barrier with increasing nanoparticle size (eq 1). Stronger fields are needed to overcome increasing magnetization reversal energy barriers; thus the coercive field increases with particle size. As the size of nanoparticles increases, the surface-to-volume ratio decreases. Therefore, the percentage of magnetic moments that are pinned on the surface decreases within the total magnetic moments of overall nanoparticles. Consequently, larger sized particles possess higher M_S and M_R values due to the per particle volume increase in the amount of magnetic moments to be aligned with the field.

Conclusions

Reverse micelle methods provide exceptional control over the composition of the $CoCr_xFe_{2-x}O_4$ nanoparticles with a reasonable size distribution. The blocking temperature, magnetic moment, and coercivity all were found to decrease with increasing Cr incorporation. Due to the weaker magnetic moment of Cr and the strong negative J_{B-B} couplings, substitution of Cr for Fe weakens the L−S couplings. The magnetic properties of the nanoparticles upon doping with Cr are consistent with a weakening of anisotropy constant K in the Stoner−Wohlfarth theory. Size dependent data for $CoCr_{0.5}Fe_{1.5}O_4$ are consistent with the size dependence of magnetic anisotropy described by the Stoner−Wohlfarth theory.

Acknowledgment. C.R.V. is partially supported by a Georgia Tech Presidential Fellowship. This work has benefited from the use of the Intense Pulse Neutron Source at Argonne National Laboratory, which is funded by the U.S. Department of Energy, BES-Materials Science under Contract No. W-31-109-ENG-38. We thank Dr. Simine Short for her assistance with neutron data collection. TEM studies were performed at the Georgia Tech Electron Microscopy Center. This research is supported in part by NSF (DMR-9875892), Sandia National Laboratory, and PECASE Program.

References and Notes

(1) Sun, S.; Murray, C. B.; Weller, D.; Folk, S. L.; Moser, A. *Science* **2000**, *287*, 1989.
(2) McMichael, R. D.; Shull, R. D.; Swaertzendruber, L. J.; Bennett, L. H. *J. Magn. Magn. Mater.* **1992**, *111*, 29.
(3) *Scientific and Clinical Applications of Magnetic Carriers*; Häfeli, U., Schütt, W., Teller, J., Zborowski, M., Eds.; Plenum: New York, 1997.
(4) Mitchell, D. G. *J. Magn. Reson. Imaging* **1997**, *7*, 1.
(5) Liu, C.; Zou, B.; Rondinone, A. J.; Zhang, Z. J. *J. Am. Chem. Soc.* **2000**, *122*, 6263.
(6) Liu, C.; Zhang, Z. J. *Chem. Mater.* **2001**, *13*, 2092.
(7) Broese Van Groenou, A.; Bergers, P. F.; Stuyts, A. L. *Mater. Sci. Eng.* **1968/69**, *3*, 317.
(8) Yafet, Y.; Kittel, C. *Phys. Rev.* **1952**, *87*, 290.
(9) Kaplan, T. A. *Phys. Rev.* **1960**, *116*, 888.
(10) Kaplan, T. A.; Dwight, K.; Lyons, D. H.; Menyuk, N. *J. Appl. Phys.* **1961**, *32*, 13S.
(11) Belov, K. P.; Goryaga, A. N.; Annaev, R. R.; Kokorev, A. I.; Lyamzin, A. N. *Sov. Phys. Solid State* **1989**, *31*, 785.
(12) Mohan, H.; Shaikh, I. A.; Kulharni, R. G. *Physica B* **1996**, *217*, 292.
(13) Goya, G. F.; Rechenberg, H. R.; Jiang, J. Z. *J. Appl. Phys.* **1998**, *84*, 1101.
(14) Chen, Q.; Rondinone, A. J.; Chakomakos, B. C.; Zhang, Z. J. *J. Magn. Magn. Mater.* **1999**, *194*, 1.
(15) Xiong, G.; Mai, Z.; Xu, M.; Cui, S.; Ni, Y.; Zhao, Z.; Wang, X.; Lu, L. *Chem. Mater.* **2001**, *13*, 1943.
(16) Pileni, M. P.; Moumen, N. *J. Phys. Chem. B* **1996**, *100*, 1867.
(17) Liu, C.; Zou, B.; Rondinone, A. J.; Zhang, Z. J. *J. Phys. Chem. B* **2000**, *104*, 2000.
(18) Vestal, C. R.; Zhang, Z. J. *Chem. Mater.* **2002**, *14*, 3817.
(19) Jorgensen, J. D.; Faber, J., Jr.; Carpenter, J. M.; Crawford, R. K.; Haumann, J. R.; Hitterman, R. L.; Kleb, R.; Ostrowski, G. E.; Rotella, F. J.; Worlton, T. G. *J. Appl. Crystallogr.* **1989**, *22*, 321.
(20) Stoner, E. C.; Wohlfarth, E. D. *Philos. Trans. R. Soc. A* **1948**, *240*, 599; reprinted in *IEEE Trans. Magn.* **1991**, *27*, 3475.
(21) Bertotti, G. *Hysteresis in Magnetism: for Physicists, Materials Scientists, and Engineers*; Academic Press: San Diego, 1998; p 157.